Earth and Planetary Science Letters 565 (2021) 116932

Contents lists available at ScienceDirect

Earth and Planetary Science Letters

www.elsevier.com/locate/epsl

The influence of hydrodynamics on the carbon isotope composition of inorganically precipitated calcite

Hao Yan [a,*], Wolfgang Dreybrodt [b], Huiming Bao [c,d], Yongbo Peng [c], Yu Wei [a], Song Ma [a], Bing Mo [e], Hailong Sun [a], Zaihua Liu [a,f,**]

[a] State Key Laboratory of Environmental Geochemistry, Institute of Geochemistry, Chinese Academy of Sciences, Guiyang 550081, China
[b] Faculty of Physics and Electrical Engineering, University of Bremen, Germany
[c] International Center for Isotope Effects Research, School of Earth Sciences and Engineering, Nanjing University, Nanjing 210023, China
[d] Department of Geology and Geophysics, Louisiana State University, Baton Rouge, LA 70803, USA
[e] Center for Lunar and Planetary Sciences, Institute of Geochemistry, Chinese Academy of Sciences, Guiyang, China
[f] CAS Center for Excellence in Quaternary Science and Global Change, 710061 Xi'an, China

ARTICLE INFO

Article history:
Received 29 July 2020
Received in revised form 17 February 2021
Accepted 2 April 2021
Available online 14 April 2021
Editor: L. Derry

Keywords:
calcite
carbon isotope fractionation
diffusion boundary layer
precipitation rate
pH effect

ABSTRACT

It is often assumed that the carbon isotope composition ($\delta^{13}C$) of carbonate minerals records that of the dissolved inorganic carbon (DIC) species with insignificant disequilibrium effect. However, results from field observations and laboratory experiments have shown that the $\delta^{13}C$ difference between calcite and solution can vary up to 3‰ even under a similar set of solution composition and temperature, raising uncertainties on the $\delta^{13}C$'s paleoclimate and paleoecology implications. One likely cause is the variable calcite precipitation rates and pH values induced by different thicknesses of the stagnant liquid layer between solid and well mixed bulk solution (i.e., diffusion boundary layer, DBL). To test this hypothesis, we selected a well-studied natural travertine deposit (Baishuitai, SW China) which consists of meter-scale travertine terraces. Calcite crystals at both the pool bottom and the rim of the terraces are inorganically precipitated from solutions identical in chemical, isotopic composition and temperature, but different only in hydrodynamics. This difference results in thicker DBL for water at the pool-bottom than for water flowing across the rim. We found that the $\delta^{13}C$ and Mg/Ca ratios are higher while Sr/Ca ratios are lower for the pool-bottom calcites than for the rim calcites. By applying a mass transfer model, we quantitatively link the differences in carbon isotope and elemental compositions of the abiogenic calcites to the different hydrodynamic conditions. The inverse variation in Mg/Ca and Sr/Ca ratios in calcites arises from the different precipitation rates between at the pool-bottom and at the rim, while the consistently lower $\delta^{13}C$ for calcites at the rim is due to their higher pH at the solid-solution interface than for calcites precipitated at the pool-bottom. In contrast, calcite precipitation rate has little influence on carbon isotope fractionation between calcite and HCO_3^-. Our results demonstrate the role of DBL thickness in governing the $\delta^{13}C$ of HCO_3^- at mineral surface, which can assist to interpret the variable $\delta^{13}C$ values of calcites in riverine or cave environments.

1. Introduction

Stable carbon isotope composition ($\delta^{13}C$) of marine and freshwater carbonates has been widely used to reconstruct the marine carbon budget (e.g., Kump and Arthur, 1999), variation in CO_2 concentration of the atmosphere (Breecker, 2017), and paleo-ecology and paleo-vegetation (e.g., Dorale et al., 1998). Combined with elemental and oxygen isotope compositions, the $\delta^{13}C$ of carbonates on land can provide specific information on, e.g., drought events (Oster et al., 2009) and monsoon variability (Zhang et al., 2011).

The foundation of these geological and environmental applications is that natural carbonates record the fluctuation of $\delta^{13}C$ values of the dissolved inorganic carbon (DIC) species in solution and this fluctuation is linked to changes in the ambient environment and/or climate. There is, however, an implicit assumption that carbon isotope fractionation between carbonate minerals and DIC ($\varepsilon_{CaCO_3/DIC}$) in solution remains constant during carbonate mineral precipitation even when there are changes in local depo-

* Corresponding author.
** Corresponding author at: State Key Laboratory of Environmental Geochemistry, Institute of Geochemistry, Chinese Academy of Sciences, Guiyang 550081, China.
E-mail addresses: yanhao@mail.gyig.ac.cn (H. Yan), liuzaihua@vip.gyig.ac.cn (Z. Liu).

https://doi.org/10.1016/j.epsl.2021.116932
0012-821X/

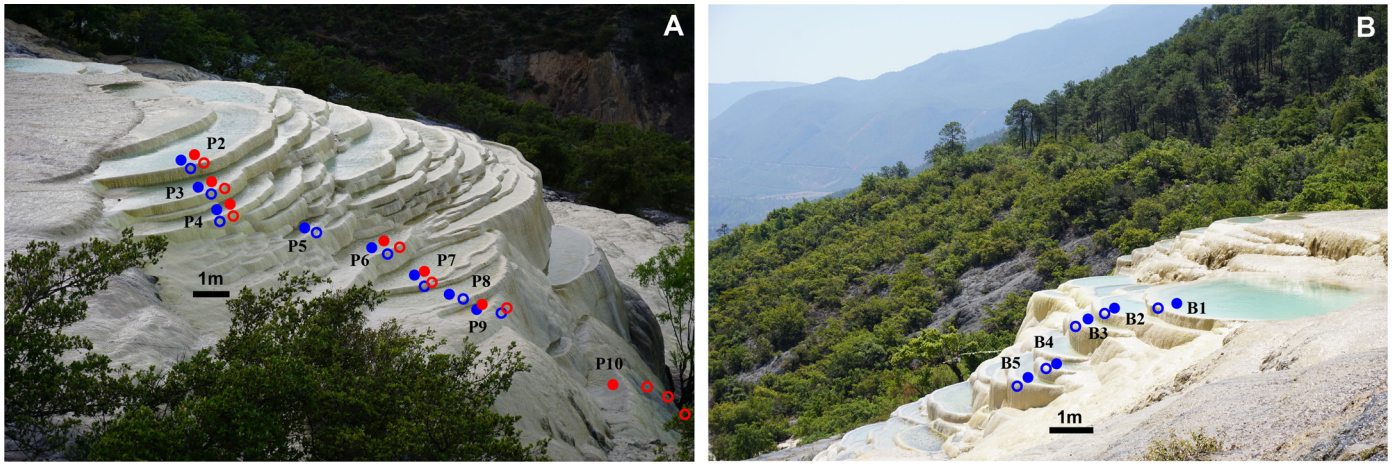

Fig. 1. Field photos of the travertine terraces at Baishuitai, SW China with the sampling sites (indicated by circles): (A) the travertine terraces for the sampling sites P*i* ($i = 2, 3, \ldots, 10$); (B) the travertine terraces for the sampling sites B*i* ($i = 1, 2, \ldots, 5$). The filled and open circles represent the sites where calcites were collected from the bottom and rim of travertine pools respectively. Two sample sets collected in February 2012 and in May 2016 are indicated by red and blue colors respectively. (For interpretation of the colors in the figure(s), the reader is referred to the web version of this article.)

sitional conditions including solution chemistry, precipitation rate, and hydrodynamics.

It has been shown that the rate of calcite precipitation influences the calcium and oxygen isotope compositions of calcite (e.g., Tang et al., 2008a; DePaolo, 2011; Watkins et al., 2014). However, it is less clear if the carbon isotope fractionation between calcite and bicarbonate ion ($\varepsilon_{calcite/HCO_3^-}$) is affected by the precipitation rate. Turner (1982) found that $\varepsilon_{calcite/HCO_3^-}$ decreased from 1.8‰ to 0.4‰ with an increase of precipitation rates in an open system where the isotope composition of the solution stayed constant. However, care must also be taken when referring to the work of Turner (1982) as he precipitated carbonates over a range of precipitation rates in a single experiment (see Fig. 8 in Romanek et al., 1992) and he precipitated a multi-mineral solid (calcite + aragonite) in some experiments. Romanek et al. (1992) performed inorganic calcite precipitation experiments with a better control of solution chemistry and precipitation rate. They reported a constant $\varepsilon_{calcite/HCO_3^-}$ value close to 1.0‰ at precipitation rates between $10^{-6.96} \sim 10^{-4.76}$ mol/m^2/s and temperatures at 10, 25 and 40 °C. Recently, Levitt et al. (2018) performed a similar set of experiments as those of Romanek et al. (1992) but at a slower calcite growth rate, and they obtained an $\varepsilon_{calcite/HCO_3^-}$ value of 1.6 ± 0.4‰. Similarly, no apparent correlation between the $\varepsilon_{calcite/HCO_3^-}$ and precipitation rates was observed in Levitt et al. (2018)'s experiments despite the fact that their precipitation rates varied over one order of magnitude. While it is difficult to synthesize in the laboratory, extremely slow-precipitated calcite from slightly supersaturated solution can be found in nature. Vein calcite from Devils Hole with growth rate on the order of 10^{-10} mol/m^2/s has an $\varepsilon_{calcite/HCO_3^-}$ value of 2.3‰ (Coplen, 2007), which is apparently higher than those from Romanek et al. (1992) and Levitt et al. (2018)'s experiments.

Theoretical model from Watkins and Hunt (2015) predicts that $\varepsilon_{calcite/HCO_3^-}$ may decrease with increasing precipitation rate when the rate is within a certain range. Their model can explain the different values of $\varepsilon_{calcite/HCO_3^-}$ between Romanek et al. (1992) and Levitt et al. (2018)'s experiments. However, the reason why there is no apparent rate dependence of $\varepsilon_{calcite/HCO_3^-}$ in individual studies is unknown.

It has been recognized that the rate of calcite precipitation is governed by ion flux at the solid-solution diffusion boundary layer (DBL), a stagnant region located between mineral surface and the well mixed bulk solution (Dreybrodt and Buhmann, 1991). Since solute transport relies on gradient-driven molecular diffusion within the DBL, the DBL thickness, controlled mainly by water flow rate over mineral surface, can affect the precipitation rate even from the same solution at the same temperature (Liu et al., 1995; Dreybrodt et al., 1997). Natural travertine dams (or terraces) with a wide range of scales, from millimeters to tens of meters, are common in caves, springs, and rivers worldwide. Their formation is attributed to an accumulative effect of different calcite precipitation/growth rates at different hydrodynamic conditions influenced by initial landscape (Hammer et al., 2007). In this study, we choose travertine terraces as a natural laboratory to study the effect of growth kinetics on $\varepsilon_{calcite/DIC}$. By comparing the $\delta^{13}C$ values of calcites precipitated at the bottom and the rim of travertine pools where the temperature and solution chemistry are identical at any time, we can assess the influence of DBL thickness on $\varepsilon_{calcite/DIC}$.

2. Geological setting

Baishuitai (N27°300′, E100°02′), Yunnan Province, SW China has one of the most spectacular travertine sceneries around the world and is the sacred site of Dongba Religion of the Naxi ethnic minority. The area is an alpine karst with a mean annual precipitation of 750 mm and an annual air temperature of 8 °C. Vegetation in this area has a distinct vertical zonation with evergreen shrubs dominant at 2200∼2500 m, *Pinus yunnanensisi* forests at 2500∼3000 m, spruce forests at 3000∼3500 m, and fir forests above 3500 m.

Baishuitai is located on Shisanjiao Mountain composed of limestones of the Triassic Beiya Formation. Due to intensive neotectonics and weathering, the limestones are highly fractured. This provides favorable conditions for rainfall infiltration and groundwater flow. Due to the cut-off by a major northwest oriented fault, groundwater resurges at an altitude of about 2550 m asl. There are two adjacent perennial springs with 10 meters distance. The two springs have identical temperature (11 °C) and water chemistry which are stable throughout the year. The hydrochemistry of spring water is of the Ca^{2+}–HCO_3^- type and features high partial pressures of CO_2 (up to 150,000 ppmv), implying an endogenic origin. After groundwater emerges, a large amount of CO_2 is released, and the aqueous solution becomes supersaturated with respect to calcium carbonate. About 200 m away from the springs, a travertine platform has formed with a thickness of several tens of meters covering an area of about 3 km^2. The platform houses numerous travertine pools (or terraces) with areas varying from 0.5 to 20 m^2 and depths from 10 to 50 cm (Fig. 1).

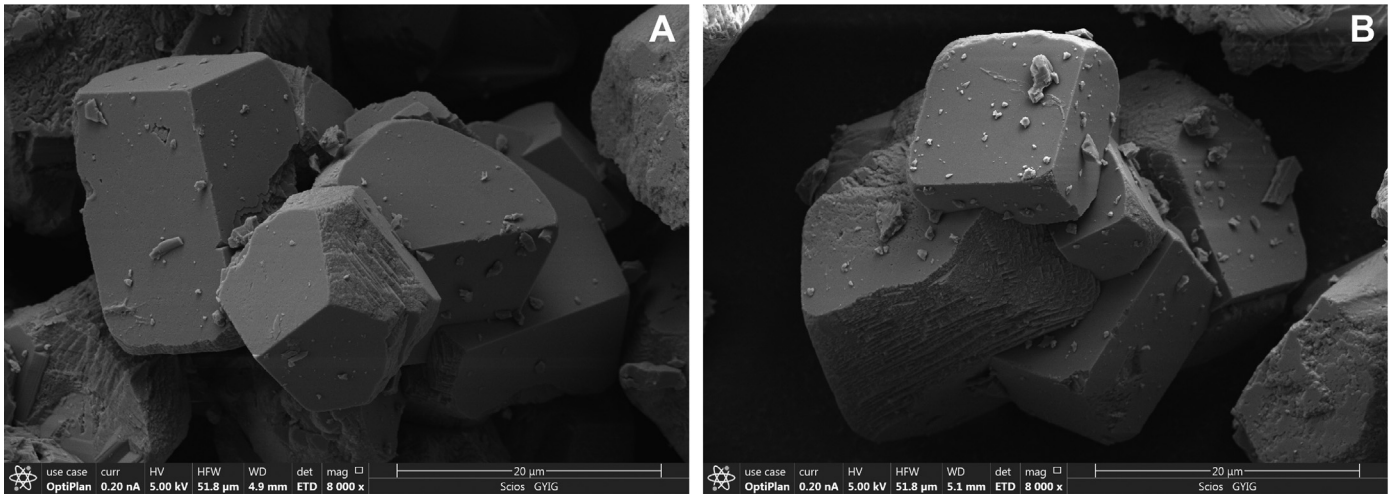

Fig. 2. SEM images of travertine calcites from (A) the bottom and (B) the rim of pool P4.

3. Materials and methods

3.1. Sampling and analysis

Fieldwork at Baishuitai was carried out in February 2012 and May 2016. Two transects were sampled along the water flow path and sample locations are shown in Fig. 1. The uppermost surface of travertine was sampled using a spatula to obtain the pristine precipitated carbonates. Back in the laboratory, samples were dried for 24 h in an oven at 60 °C and then stored in centrifuge tubes for further analyses. Water samples for carbon isotope composition of DIC were collected by a syringe with 0.45 µm filter and stored in a 15 mL pre-cleaned glass vial with no air bubbles or headspace. One drop of saturated $HgCl_2$ solution was added to each sample to prevent microbial activity. All samples were kept at 4 °C until isotopic measurements. Water temperature (T), pH, and electrical conductivity (EC) were measured with a hand-held water quality meter (WTW 350i) with accuracies of ±0.1 °C, ±0.05 pH unit, and ±0.5%, respectively. Alkalinity and concentration of Ca^{2+} ($[Ca^{2+}]$) were titrated on-site using Aquamerck® Alkalinity Test and Hardness Test with resolutions of 0.1 mmol/L and 2 mg/L, respectively.

All laboratory work including SEM observations, elemental analyses, and stable isotope measurements was conducted in the Institute of Geochemistry, Chinese Academy of Sciences (IGCAS). Several travertine samples were analysed by X-Ray Diffraction (XRD) and scanning electron microscope (SEM) to examine the mineralogy and inorganic growth feature of carbonate crystals. Ca, Sr, and Mg contents in travertine carbonate collected in February 2012 were analysed using an inductively coupled plasma optical emission spectrometer (ICP-OES, Vista MPX, USA) with a precision of better than 5%. Isotopic measurements of travertine and DIC were performed in a continuous-flow mode using a MAT 253 isotope ratio mass spectrometry (IRMS) equipped with GasBench II (Thermo Scientific™) for acid digestion. The results are reported relative to Vienna Pee Dee Belemnite (VPDB). The reproducibility of isotopic measurements is better than ±0.1‰ for $\delta^{13}C$ based on repeated measurements of international standards NBS-18, NBS-19, and laboratory standards. The carbon isotope fractionation between A and B is expressed as:

$$\varepsilon_{A/B} = 1000(\alpha_{A/B} - 1) \quad (1)$$

where A and B are the species of a carbonate system, such as CO_2, HCO_3^-, CO_3^{2-}, and $CaCO_3$. $\alpha_{A/B}$ is carbon isotope fractionation factor between A and B and can be calculated from the $\delta^{13}C$ values of A and B:

$$\alpha_{A/B} = \frac{^{13/12}R_A}{^{13/12}R_B} = \frac{\delta_A + 1000}{\delta_B + 1000} \quad (2)$$

where δ_A and δ_B are in per mil (‰).

3.2. Calculation of the $\delta^{13}C$ value of HCO_3^-

The $\delta^{13}C$ value of HCO_3^- ($\delta^{13}C_{HCO3}$) is calculated from the $\delta^{13}C$ value of DIC ($\delta^{13}C_{DIC}$), the relative fraction of $CO_{2,aq}$, HCO_3^-, and CO_3^{2-}, and the equilibrium isotope fractionation factors between $CO_{2,aq}$ and HCO_3^- ($\alpha^{eq}_{HCO_3^-/CO_{2,aq}}$) and between HCO_3^- and CO_3^{2-} ($\alpha^{eq}_{HCO_3^-/CO_3^{2-}}$). Here, we use PHREEQC program (Parkhurst and Appelo, 1999) to calculate the relative fraction of DIC species with the data of water temperature, pH, alkalinity, and $[Ca^{2+}]$. $\alpha^{eq}_{HCO_3^-/CO_{2,aq}}$ and $\alpha^{eq}_{HCO_3^-/CO_3^{2-}}$ are from Mook et al. (1974) and Turner (1982).

4. Results

XRD results reveal that calcite is the only phase in travertine carbonates at Baishuitai, consistent with the results of Yan et al. (2016). Fig. 2 shows the SEM images of travertine calcite crystals collected from the bottom and rim of site P4 in May 2016. No macroscopic algal filament or biofilm is observed between crystals, indicating that rhombohedral calcite originated primarily from inorganic precipitation.

The carbon isotope compositions of travertine calcites ($\delta^{13}C_{calcite}$) from the bottom and the rim of pools are displayed in Fig. 3 (see supplementary material for the raw data). The $\delta^{13}C$ of calcite is consistently lower at the rim than that at the bottom of the same pool (Fig. 3). The difference between the paired sites ($\delta^{13}C_{rim} - \delta^{13}C_{bottom}$) is -0.49 ± 0.10‰ while the $\delta^{13}C$ of DIC at the paired sites are the same within analytical error. Carbon isotope fractionation between calcite and DIC ($\varepsilon_{calcite/DIC}$) at the bottom and the rim are 1.93 ± 0.08‰ and 1.54 ± 0.12‰ respectively. At pH values of 8.02 to 8.15, more than 97% of DIC is HCO_3^-. In this case, $\delta^{13}C_{HCO3}$ is only ~0.2‰ higher than $\delta^{13}C_{DIC}$. Thus, the apparent $\varepsilon_{calcite/HCO_3^-}$ at the bottom and the rim are 1.71 ± 0.08‰ and 1.33 ± 0.11‰ respectively. For the $\delta^{18}O$ of calcite, however, we found no difference between the pool bottom and the rim sites ($\delta^{18}O_{rim} - \delta^{18}O_{bottom} = -0.07 \pm 0.20$‰, Table S1). The Mg/Ca and Sr/Ca ratios in these calcites are also characterized by saw-toothed

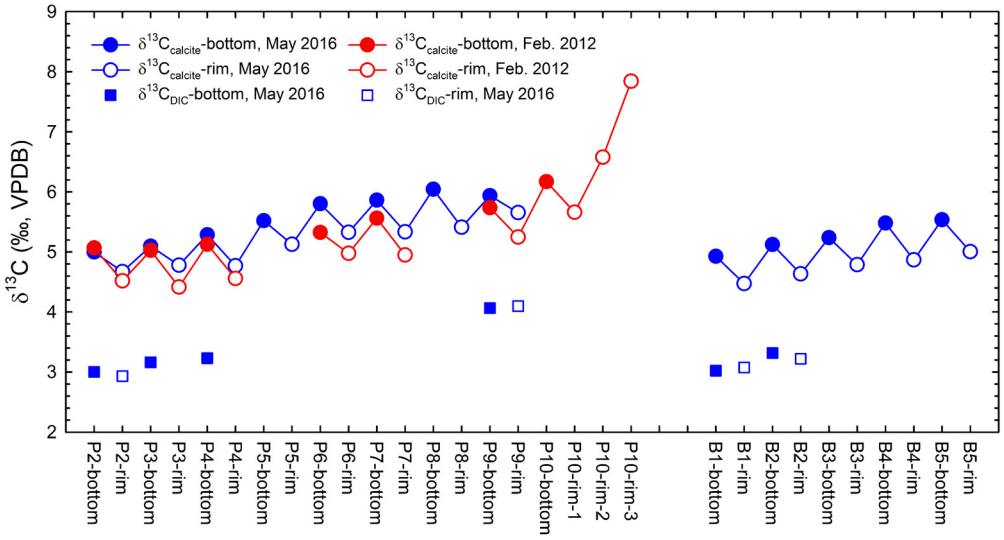

Fig. 3. Spatial variation in $\delta^{13}C$ values of calcite and of DIC in the solution along the travertine terraces.

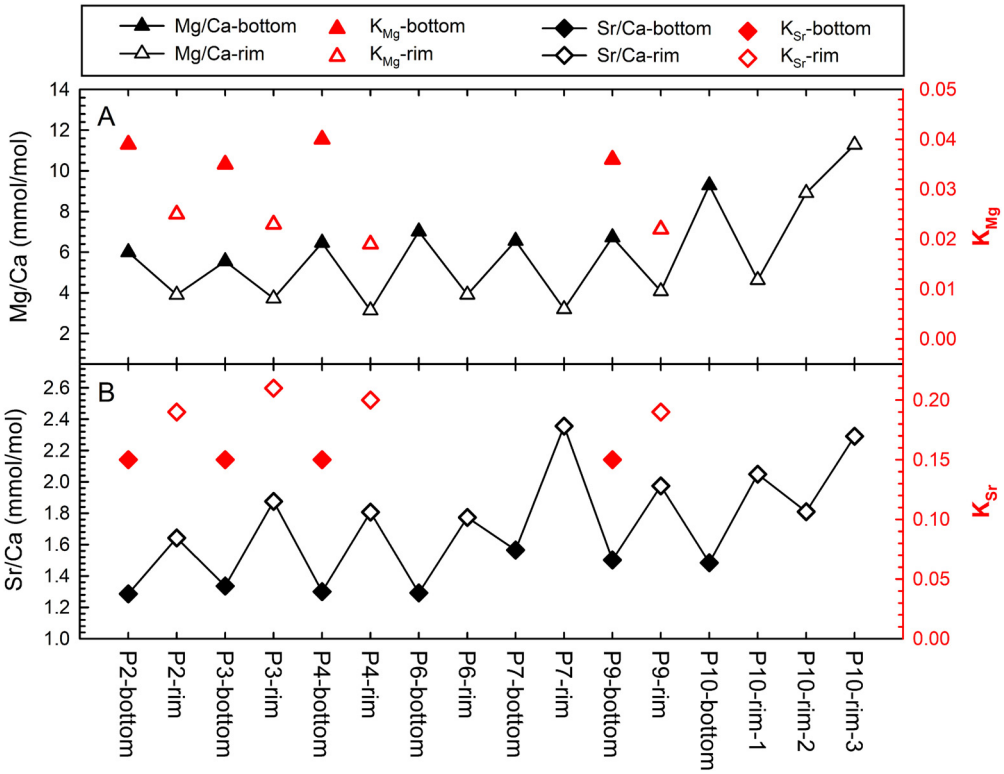

Fig. 4. Spatial variation in (A) Mg/Ca ratios of calcite and the associated K_{Mg}, (B) Sr/Ca ratios of calcite and the associated K_{Sr} along travertine terraces. The travertine calcites were sampled in February 2012.

pattern (black lines in Fig. 4). However, the Mg/Ca and Sr/Ca ratios vary inversely, i.e., higher Mg/Ca and lower Sr/Ca ratios occur in bottom calcites than those in rim calcites. The average Mg/Ca and Sr/Ca ratios in calcites are 6.80 mmol/mol and 1.40 mmol/mol at the pool bottom, 3.80 mmol/mol and 1.93 mmol/mol at the rim, respectively. Spatially, a gradual increase in $\delta^{13}C_{calcite}$ values is observed along each transect (Fig. 3), which has been explained in a previous study by a preferential removal of ^{12}C from the solution during CO_2 degassing (Yan et al., 2020). In contrast, no obvious downstream trend is found for the Mg/Ca and Sr/Ca ratios (Fig. 4).

5. Discussion

5.1. Identical chemical and isotopic compositions of bulk solutions at the bottom and the rim

Results of mineralogical analyses show that calcite is the only phase for carbonates precipitated at the bottom and the rim of travertine pools and there is no difference in crystal size or growth features between the two settings. Thus, the influence of mineralogy on elemental partitioning and carbon isotope fractionation can be excluded.

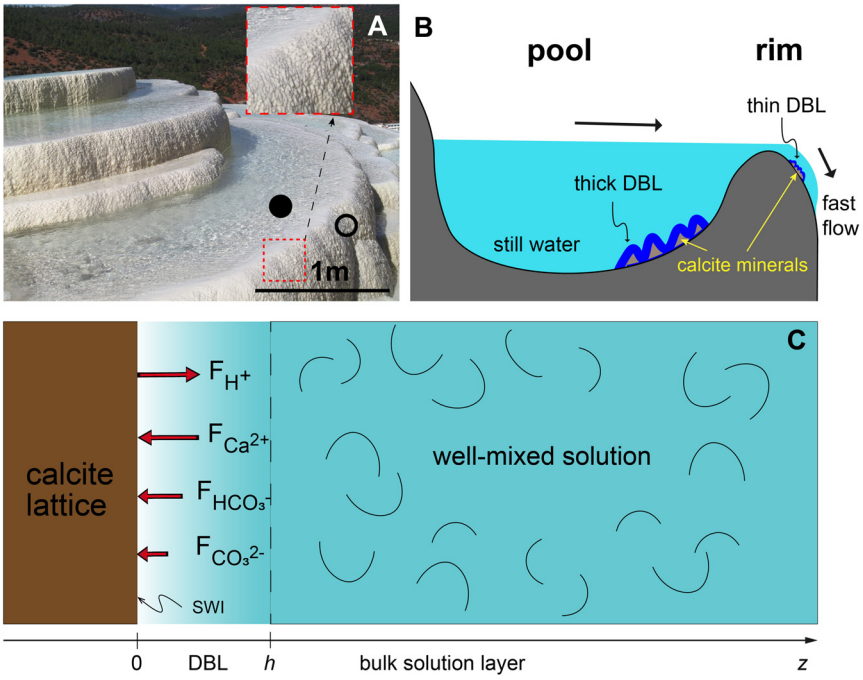

Fig. 5. (A) Field photos of travertine pool P4. The locations for calcite collection at the pool bottom and the rim are indicated by solid and open circle respectively. Inside the red dashed square is the close-up of the rough rim of the travertine pool. (B) Sketch of hydrodynamic controls on the thickness of diffusion boundary layer (DBL) on the surface of calcite minerals. (C) Illustration of $CaCO_3$–H_2O–CO_2 system with well mixed bulk solution and a diffusion boundary layer (modified from Dreybrodt and Buhmann, 1991). h is the thickness of the DBL.

Another factor that could cause the observed $\delta^{13}C_{calcite}$ difference in the two settings is that the chemical and isotopic compositions of bulk solutions at the bottom and the rim of travertine pools are different. This difference in [DIC] ($\Delta C = C_{bott} - C_{rim}$) between the paired sites is linked to the amount of DIC removed by calcite precipitation and CO_2 degassing when water flows from the pool bottom to the rim. From mass balance one gets (see Appendix A for derivation)

$$\Delta C = \frac{2R_p \times l}{v_{rim} \times d_{rim}} \tag{3}$$

where R_p is the precipitation rate of calcite; the factor 2 denotes the rate of DIC removed from the solution is twice the precipitation rate required by stoichiometry; l is the distance between the bottom and rim sites; v_{rim} is the flow velocity at the rim; d_{rim} is the water depth at the rim. Given $R_p < 2 \times 10^{-6}$ mol/m^2/s (see Section 5.2), $l < 0.3$ m, $v_{rim} > 0.01$ m/s, and $d_{rim} \approx 0.005$ m, ΔC is smaller than 0.02 mmol/L. This conclusion is consistent with the observations of Liu et al. (1995) who found no measurable difference of pH and electrical conductivity in solutions between at the bottom and at the rim of travertine pools at Huanglong Ravine, China. Our data also show that the bulk solutions at the bottom and at the rim exhibit the same $\delta^{13}C_{DIC}$ value within analytical error.

5.2. Different DBL thicknesses between at the bottom and the rim of travertine pools

With mineralogy, crystal size, and solution chemistry being excluded as potential causes of the observed $\varepsilon_{calcite/DIC}$ difference between the bottom and the rim sites, we must examine the difference in transport dynamics at the microscopic level caused by different thicknesses of DBL on the surface of calcite crystals between the two settings. Calcite precipitation from a Ca^{2+}–HCO_3^- solution will consume Ca^{2+} and CO_3^{2-} and produce H^+, resulting in solution chemistry at the mineral surface being different from that in the bulk solution (Fig. 5). The existence of a DBL generates a transfer resistance for these ions, thus strongly reducing the precipitation rates of calcite (Buhmann and Dreybrodt, 1985). Dreybrodt and his co-workers have suggested that precipitation rates can vary by as much as one order of magnitude given different thicknesses of DBL even when bulk solution composition remains constant (Buhmann and Dreybrodt, 1985; Dreybrodt and Buhmann, 1991; Dreybrodt, 2012). In this study, a large difference in DBL thickness is caused by the distinct hydrodynamic conditions at the bottom and the rim of the pools, which is illustrated in Fig. 5. The nearly still water at the bottom generates thick DBLs whereas fast flow at the rim results in thin layers.

The thickness of a DBL is typically on the order of tens of microns to millimeters, depending on the nature and roughness of the substrate, as well as on the flow velocity of the overlying water (Dreybrodt et al., 1992; Boudreau and Jørgensen, 2001; Han et al., 2018; Sulpis et al., 2019). Accurate estimation of DBL thickness is difficult, especially for the solution flowing on a rough surface (Han et al., 2018). Jørgensen and Revsbech (1985) determined the thickness of DBLs by micrometer-scale electrodes and found the DBLs are 0.2∼1.0 mm thick for lake and ocean environments. Sulpis et al. (2019) reported a DBL thickness of about 0.5 mm under the condition of the rotation rate of 1 rpm in their rotating disc experiments, representative of low-energy aquatic natural environments. In this study, we choose 0.5 mm as the DBL thickness for our pool bottom calcites. In fact, the following interpretation will hold when the DBL thickness at the pool bottom is within the range of 0.2 and 0.5 mm because when DBL is thicker than 0.2 mm, further increase in thickness has little influence on the precipitation rate as reactions occurring within the DBL determine the CO_3^{2-} fluxes at the mineral surface (Dreybrodt and Buhmann, 1991). DBL thickness in a turbulent flow can be estimated using gypsum dissolution which is controlled entirely by mass diffusion (Dreybrodt et al., 1992). Using this method, Liu et al. (1995) determined the DBL thickness at the rimstone dams at Huanglong Ravine to be 0.1 ± 0.04 mm. However, in their study the theoretical precipitation rates were much lower than the measured ones at the two

last sites with high turbulence, indicating that the real DBL thickness there was smaller than 0.1 mm. Considering a much thicker (>3 cm) water flow at the rimstone dams in Liu et al.'s study than that (<0.5 cm) at the rim of pools in this study (for more details, see section 5.4), DBL thickness of 0.05 mm is chosen for the rim conditions in the subsequent discussion.

With the estimated values of DBL thickness and the chemistry of bulk solution (Table S2), we calculated the precipitation rates of calcite at the bottom and the rim of travertine pools by employing the DBL model developed by Dreybrodt and Buhmann (1991). This model considers the combination of three processes, i.e., kinetics of the heterogeneous growth of calcite, kinetics of the conversion of HCO_3^- to CO_2, and mass transport by diffusion. Basically, the concentrations of ions (i.e., Ca^{2+}, HCO_3^-, CO_3^{2-} and H^+) across the DBL can be described by the following system of partial differential equations:

$$\frac{\partial C_i(t,z)}{\partial t} = D_i \frac{\partial^2 C_i(t,z)}{\partial z^2} + R_i \tag{4}$$

where $C_i(t,z)$ denotes the concentration of species i (i.e., $CO_{2,aq}$, HCO_3^-, CO_3^{2-}, Ca^{2+} and H^+) at time t and distance z from solid-water interface (Fig. 5c), D_i is the diffusion coefficient of species i, and R_i is the net reaction rate of species i. The above formula can be solved by iterative methods (see Dreybrodt and Buhmann, 1991; Guo and Zhou, 2019, for the details of calculation). The precipitation rates of calcite are then calculated using the Plummer-Wigley-Parkhurst (PWP) equation (Plummer et al., 1978) as:

$$R_p = \kappa_4 (HCO_3^-)_0 (Ca^{2+})_0 - \kappa_1 (H^+)_0 - \kappa_2 (H_2CO_3^*)_0 - \kappa_3 \tag{5}$$

where κ_1, κ_2, and κ_3 are temperature dependent kinetic reaction constants, while κ_4 also depends on the activity $(H_2CO_3^*)_0$; the brackets denote the activity of each species; the subscript 0 means $z = 0$, i.e., at the mineral surface. The calculated precipitation rates fall in the range of 5.2×10^{-7} to 6.6×10^{-7} mol/m^2/s at the bottom and 1.3×10^{-6} to 1.8×10^{-6} mol/m^2/s at the rim (Table S2). The calculated values at the bottom are consistent with the measured rates of newly precipitated calcites on substrates in the field ($5.86 \pm 1.66 \times 10^{-7}$ mol/m^2/s, $n = 5$, Yan et al., 2016), indicating the validity of the DBL thickness of 0.5 mm at the pool bottom. No direct measurement of precipitation rate has been performed at the rim because the water film there is too thin to place a substrate. However, our calculation shows the precipitation rates at the rim are ~2.6 times higher than those at the pool bottom, which is comparable to the results of Liu et al. (1995) who found the precipitation rates at the rimstones 2~5 times higher than inside the pools at Huanglong Ravine.

Since the temperature and chemistry of bulk solution at the paired sites of a pool are demonstrated to be identical in section 5.1, the regular variation in Mg/Ca and Sr/Ca ratios in calcite along a flow path (Fig. 4) is likely the result of different precipitation rates owing to distinct hydrodynamics at the two depositional settings. Inverse variation patterns of Mg/Ca and Sr/Ca ratios in calcites along travertine terraces imply the opposite responses of Mg/Ca and Sr/Ca partitioning to changing precipitation rate (Gabitov et al., 2014). Although no consensus has been achieved on the effect of precipitation rate on *Me*/Ca partitioning (*Me* denotes Mg or Sr) between calcite and parent solution (e.g., Mucci and Morse, 1983; Tang et al., 2008b; Mavromatis et al., 2013; Gabitov et al., 2014), Mg/Ca and Sr/Ca partition coefficients are found to vary with precipitation rate in some abiotic calcite-precipitated experiments (e.g., Tang et al., 2008b; Gabitov et al., 2014). Here, we use Mg/Ca and Sr/Ca ratios in calcites from the bottom and the rim to further evaluate the rationality of the estimated DBL thickness. As aqueous samples for Mg^{2+} and Sr^{2+} concentrations ($[Mg^{2+}]$ and $[Sr^{2+}]$) at the bottom-rim sampling sites were not collected, Mg^{2+} and Sr^{2+} concentrations in spring water from previous studies (Yan et al., 2012, 2016) are adopted in this study to calculate the partition coefficients, which brackets the uncertainty of calculated partition coefficients to less than 2% and 5% for Mg/Ca and Sr/Ca respectively. Using the concentrations of Ca^{2+} in several pools, we calculate the partition coefficients of Mg^{2+} and Sr^{2+} by assuming the solutions at the paired sites of a pool have the identical Mg^{2+}, Sr^{2+} and Ca^{2+} concentrations (Fig. 4, Table S3). The equation for partition coefficients (K_{Me}) is expressed as $K_{Me} = (Me/Ca)_{calcite}/(Me/Ca)_{fluid}$ (Gabitov et al., 2014). The values of K_{Mg} and K_{Sr} are 0.037 ± 0.002 and 0.15 ± 0.00 at the bottom and 0.022 ± 0.003 and 0.20 ± 0.01 at the rim of the pools, respectively (Fig. 4). The absolute values and rate dependences of K_{Mg} and K_{Sr} agree well with the estimations by employing the relationships proposed by Gabitov et al. (2014) and Tang et al. (2008b) respectively. Such an agreement, in turn, implies that our chosen values of DBL thickness for calculation of precipitation rate are valid.

5.3. Interpreting the variations in $\delta^{13}C_{calcite}$ at Baishuitai travertine terraces

As both pH and precipitation rate may have an impact on the apparent isotope fractionation between DIC and calcite, we must determine which process plays the dominant role. Despite no consensus on the dependence of $\varepsilon_{calcite/HCO_3^-}$ on calcite precipitation rate, ion-by-ion growth model predicts a significant negative correlation between $\varepsilon_{calcite/HCO_3^-}$ and precipitation rate within the range of 10^{-7} mol/m^2/s $< R_p <$ 10^{-5} mol/m^2/s (see Fig. 3 in Watkins and Hunt, 2015) which covers the range of precipitation rates in this study. Alternatively, the $\delta^{13}C_{calcite}$ difference between the pool bottom and the rim sites may be the result of different $\delta^{13}C_{HCO3}$ in the interface solutions owing to the pH-dependence of the relative abundance of DIC species. As stated above, due to the existence of a DBL, pH at the mineral-solution interface could be quite different from that of the bulk solution.

Here we calculate pH and ion concentrations (e.g., Ca^{2+}, HCO_3^-, CO_3^{2-}) at the solid-water interface using Equation (4). The profiles of pH and $[CO_3^{2-}]$ across the DBL are shown in Fig. 6 for a bulk solution of $[Ca^{2+}] = 4$ mmol/L and pH = 8.1 when DBL thickness (h) is 0.5 mm and 0.05 mm respectively. Both pH and $[CO_3^{2-}]$ are much lower at the mineral-solution interface than in the bulk solution. Note that $[CO_3^{2-}]$ is not a linear function of the distance from the interface at $h = 0.5$ mm because the conversion of HCO_3^- to CO_2 within the DBL becomes significant when this layer is sufficiently thick, i.e., >0.2 mm (Dreybrodt and Buhmann, 1991). In contrast, $[Ca^{2+}]$ and $[HCO_3^-]$ have little variations across the DBL.

The calculated results for pH at the mineral surface at the pool bottom and rim sites at Baishuitai are given in Table S2. Despite having the same bulk solution pH for the paired sites, pH at the mineral surface for $h = 0.5$ mm at the pool bottom is about 0.15 lower than that for $h = 0.05$ mm at the rim. When pH is at 7, dissolved CO_2 accounts for more than 10% of DIC while the fraction of CO_3^{2-} is negligible. Under this circumstance, a small change in pH will lead to a very different $\delta^{13}C_{HCO3}$ value due to the large carbon isotope fractionation between $CO_{2,aq}$ and HCO_3^- (10.14‰ at 15 °C, Mook et al., 1974). According to our calculation, 16% of DIC at the mineral surface is $CO_{2,aq}$ for the pool bottom sites, while only 12% is $CO_{2,aq}$ for the rim sites. And this difference in the fraction of $CO_{2,aq}$ in DIC between the paired sites (16% vs. 12%) can cause a difference in $\delta^{13}C_{HCO3}$ of 0.41‰ at the mineral surface, which is close to the $\delta^{13}C_{calcite}$ difference of 0.49 ± 0.10‰ observed between the paired sites. Such an agreement implies that local equilibrium among DIC species, rather than kinetic effect of

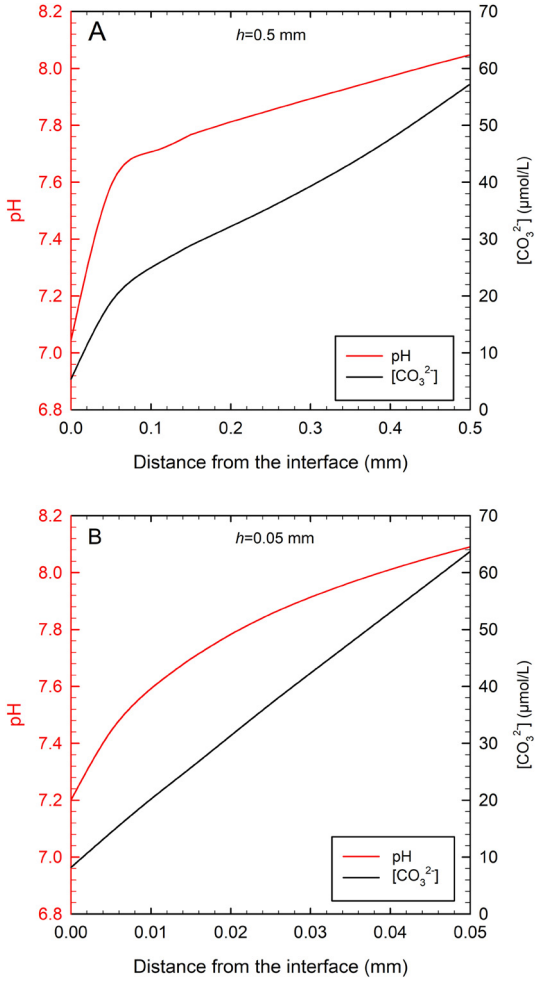

Fig. 6. Profiles of pH and CO_3^{2-} across the diffusion boundary layer for (A) $h =$ 0.5 mm at the bottom, (B) $h = 0.05$ mm at the rim, when pH and $[Ca^{2+}]$ of the bulk solution are 8.1 and 4 mmol/L, respectively, which represents the average conditions of travertine pools in this study. For simplicity, $[HCO_3^-] = 2[Ca^{2+}]$.

faster calcite precipitation at the rim, mainly contributes to the consistently low $\delta^{13}C_{calcite}$ values at the rim.

It should be noted that there are two assumptions in the deduction above. One is that the $\delta^{13}C_{DIC}$ at the mineral surface is identical to that in the bulk solution. This assumption holds because transport of DIC to the mineral surface across the DBL is driven by ion diffusion with negligible isotope fractionation (Zeebe, 2011). The other assumption is that carbon isotopic equilibrium among DIC species has reached before HCO_3^- and CO_3^{2-} are incorporated into crystal lattice. According to the calculation by Zeebe et al. (1999), the relaxation time for carbon isotopic equilibrium among DIC species (τ_{eq}^{C}) is 17.5 s at pH 8.2 at 25 °C. In comparison, the time constant for calcite precipitation (τ_{pr}), depending on the thickness of water, is much larger. For the water thickness of 0.3∼3 cm, τ_{pr} ranges from 1000 s to 10^4 s at 20 °C (Dreybrodt and Scholz, 2011). Thus, it is safe to assume that carbon isotopic equilibrium among DIC species is attained at the mineral surface. For oxygen isotopes, the time constant for isotopic equilibrium between DIC species and H_2O (τ_{eq}^{O}) is about 10^4 s at pH = 8.3 and $T = 20$ °C (Beck et al., 2005; Dreybrodt and Scholz, 2011), on the same magnitude of τ_{pr}. For pH ≈ 7, τ_{eq}^{O} should be smaller due to the higher concentration of $CO_{2,aq}$ in DIC. Thus, we speculate that oxygen isotope compositions of HCO_3^- and CO_3^{2-} at the mineral surface for incorporation are buffered via isotope exchange with the overwhelming H_2O. There is no isotope re-balance for oxygen as there is for carbon among carbon-bearing species at the

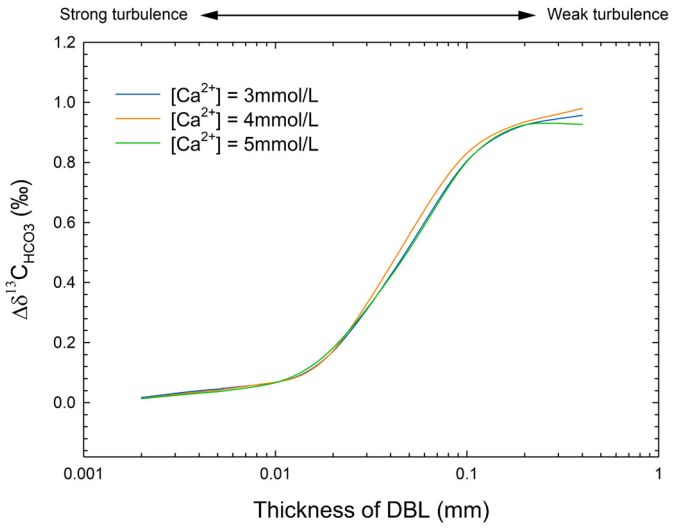

Fig. 7. The $\delta^{13}C_{HCO3}$ difference between at the mineral-solution interface and in the bulk solution ($\Delta\delta^{13}C_{HCO3}$) as a function of DBL thickness under the conditions of $T = 20$ °C, pH = 8.3, and various concentrations of Ca^{2+}.

mineral-solution interface. This could explain why there is a consistent shift in $\delta^{13}C_{calcite}$ but no obvious difference in $\delta^{18}O_{calcite}$ between the pool bottom and rim sites.

Our finding implies that, for elements such as boron whose partition of different aqueous species is sensitive to pH, the DBL thickness which has an influence on the pH at the mineral surface must be considered when interpreting their isotope data. In addition, our results support the conclusion in Romanek et al. (1992)'s study that calcite precipitation rate has negligible influence on carbon isotope fractionation between calcite and HCO_3^-.

5.4. The influence of DBL thickness on $\delta^{13}C_{calcite}$ and its implications

Using Equation (4) and the carbon isotope fractionation factors from Mook et al. (1974) and Turner (1982), we calculated the solution $\delta^{13}C_{HCO3}$ difference ($\Delta\delta^{13}C_{HCO3}$) between at the solid-water interface solution and in the bulk solution as a function of DBL thickness under the conditions of $T = 20$ °C, pH = 8.3, and various concentrations of Ca^{2+}, which represents the typical Ca^{2+}–HCO_3^--type solutions in nature. Our results show that, as the DBL gets thicker, HCO_3^- at the mineral surface become more enriched in ^{13}C than that in the bulk solution (Fig. 7). The most rapid increase in $\Delta\delta^{13}C_{HCO3}$ takes place when DBL thickness h increases from 0.02 to 0.2 mm. Concentration of Ca^{2+} shows negligible effect on $\Delta\delta^{13}C_{HCO3}$.

The effect of DBL thickness on $\delta^{13}C_{HCO3}$ at the mineral surface offers a probable explanation for the observed large $\varepsilon_{calcite/DIC}$ variability in riverine or cave calcite-depositing environments (Riechelmann et al., 2013; Zavadlav et al., 2017; EL-Shenawy et al., 2020). Depending on the flow velocity and topography of the substrates, DBL thickness in riverine environments varies greatly. According to field measurements by Dreybrodt et al. (1992), sediment-water DBL thickness is between 0.1 mm and 0.3 mm in a calcite-depositing stream where flow velocity ranges from 0.33 to 1.33 m/s. Previous studies have shown that apparent $\varepsilon_{calcite/DIC}$ values in riverine systems often fall between 1.5‰ and 2.5‰ (e.g., Lojen et al., 2009; Osácar et al., 2016; Zavadlav et al., 2017), close to the $\varepsilon_{calcite/HCO_3^-}$ values for slow-precipitated calcites in Devils Hole (Coplen, 2007).

As the overlying water becomes thinner, centimeter-scale micro-terraces are observed, which increase the roughness of the substrate significantly as shown at the rim setting in Fig. 5A. The effects of bed roughness on solute transfer from the overlying wa-

ter to sediment beds have recently been quantified by Han et al. (2018) using Large Eddy Simulation (LES) technique. Their results show that, as the substrates change from a smooth regime to a rough regime, the solute transfer coefficient is greatly enhanced. Under the rough regime, the solute transfer coefficient correlates inversely with water depth in the form of a power law (Han et al., 2018). Thus, in the environments where thin water flows on a rough bed like the rim of travertine pools at Baishuitai, the DBL may be much thinner than in a riverine environment of the same flow velocity (Dreybrodt et al., 1992), resulting in a lower apparent $\varepsilon_{\text{calcite/DIC}}$ value (1.5 ± 0.1‰) at the rim sites.

Compared with riverine/stream environment, the studies on apparent $\varepsilon_{\text{calcite/DIC}}$ in caves are limited due to the difficulties of water sampling. In cave pool settings, the mineral-solution DBL has a thickness similar to those in travertine pools. EL-Shenawy et al. (2020) simulated the formation of speleothems in an artificial cave and obtained an apparent $\varepsilon_{\text{calcite/DIC}} = 1.7 \pm 0.7$‰ in the pool-like settings, close to the values from the pool bottom in this study. Under the stalagmite-growth condition, water film on the stalagmite surface is laminar or stagnant. Baker (1993) measured the thickness of the water film on the stalagmite cap to be 0.045 ± 0.019 mm, using a vernier spherometer. Mickler et al. (2006) collected newly precipitated stalagmite calcites in Harrison's Cave (Barbados) by placing glass plates underneath the drip sites. They found the $\delta^{13}C$ of calcites in center of the plates is ~1.0‰ higher than that of DIC in the drip water. In the same way, Riechelmann et al. (2013) collected fresh calcites in Bunker Cave (Germany) and observed a difference of 1.0 ± 0.5‰ between $\delta^{13}C_{\text{calcite}}$ and $\delta^{13}C_{\text{dripwater}}$ at high drip rates >10 drops/min. The above values are close to the $\varepsilon_{\text{calcite/HCO}_3^-}$ values calibrated by Romanek et al. (1992)'s experiments in which the solutions were vigorously stirred and the mineral-solution DBLs were thin.

It should be noted that kinetic isotope fractionation during precipitation-associated degassing of CO_2 (Dreybrodt, 2019; Yan et al., 2020) can increase the $\delta^{13}C_{\text{calcite}}$, thus enlarging the apparent difference between $\delta^{13}C_{\text{calcite}}$ and $\delta^{13}C_{\text{DIC}}$ of the drip water. For instance, Riechelmann et al. (2013) obtained a difference between $\delta^{13}C_{\text{calcite}}$ and $\delta^{13}C_{\text{dripwater}}$ of 3.0 ± 0.7‰ at low drip rate <0.1 drops/min.

6. Conclusion

We found a consistently lower $\delta^{13}C$ and Mg/Ca ratio but higher Sr/Ca ratio in calcites from the rim in comparison with those from the bottom of travertine pools (Baishuitai, SW China) where bulk solutions have identical chemistry and temperature. We reduced the apparent difference in hydrodynamics in the two settings to one factor: the thickness of mineral-water diffusion boundary layer.

In the framework of Dreybrodt and Buhmann's DBL model (1991), we show that different DBL thicknesses result in different pH on the mineral surface, inducing different carbon isotope and elemental compositions of calcites even when precipitating from the same bulk solution. In general, stiller waters have thicker DBLs and result in lower pH on the mineral surface, which drives the apparent $\varepsilon_{\text{calcite/DIC}}$ values higher. Our findings provide a mechanistic interpretation on the variability of the observed $\varepsilon_{\text{calcite/DIC}}$ in riverine or cave environments.

CRediT authorship contribution statement

Hao Yan: Conceptualization, Methodology, Software, Writing – Original draft preparation. **Wolfgang Dreybrodt:** Data curation, Writing – Original draft preparation. **Huiming Bao:** Writing – Review & Editing, Visualization. **Yongbo Peng:** Investigation, Writing – Review & Editing. **Yu Wei:** Investigation. **Song Ma:** Investigation. **Bing Mo:** Investigation. **Hailong Sun:** Investigation. **Zaihua Liu:** Supervision, Funding acquisition.

Declaration of competing interest

The authors declare that they have no known competing financial interests or personal relationships that could have appeared to influence the work reported in this paper.

Acknowledgements

We would like to thank Haiyang Luo for discussion. We also thank Editor-in-Chief Dr. Louis Derry, Dr. Chris Romanek and an anonymous reviewer for detailed and constructive comments that helped us to improve the manuscript significantly. This study was supported by the Strategic Priority Research Program of Chinese Academy of Sciences, China (Grant No. XDB40000000, XDB18010104), the National Natural Science Foundation of China, China (Grant Nos. 41673019, U1612441 and 41921004).

Appendix A. Derivation of Equation (3)

Considering mass balance, one gets

$$Q \times \Delta C = 2R_p \times A \tag{A.1}$$

where Q is the amount of flow passing the rim with a width of w and A is the surface area on that calcite is deposited. Thus,

$$Q = v_{\text{rim}} \times d_{\text{rim}} \times w \tag{A.2}$$

$$A \approx l \times w \tag{A.3}$$

where v_{rim} and d_{rim} are the flow velocity and the depth of the water across the rim respectively, and l is the distance between the bottom and rim sites.

Substituting Equation (A.2) and (A.3) into Equation (A.1), one gets

$$\Delta C = \frac{2R_p \times l}{v_{\text{rim}} \times d_{\text{rim}}} \tag{A.4}$$

Appendix B. Supplementary material

Supplementary material related to this article can be found online at https://doi.org/10.1016/j.epsl.2021.116932.

References

Baker, A., 1993. Speleothem growth rate and palaeoclimate. Ph.D. Thesis. Univ. Bristol.
Beck, W.C., Grossman, E.L., Morse, J.W., 2005. Experimental studies of oxygen isotope fractionation in the carbonic acid system at 15°, 25°, and 40 °C. Geochim. Cosmochim. Acta 69 (14), 3493–3503.
Boudreau, B.P., Jørgensen, B.B., 2001. The Benthic Boundary Layer: Transport Processes and Biogeochemistry. Oxford University Press.
Breecker, D.O., 2017. Atmospheric pCO_2 control on speleothem stable carbon isotope compositions. Earth Planet. Sci. Lett. 458, 58–68.
Buhmann, D., Dreybrodt, W., 1985. The kinetics of calcite dissolution and precipitation in geologically relevant situations of karst areas: 1. Open system. Chem. Geol. 48, 189–211.
Coplen, T.B., 2007. Calibration of the calcite–water oxygen-isotope geothermometer at Devils Hole, Nevada, a natural laboratory. Geochim. Cosmochim. Acta 71, 3948–3957.
DePaolo, D.J., 2011. Surface kinetic model for isotopic and trace element fractionation during precipitation of calcite from aqueous solutions. Geochim. Cosmochim. Acta 75, 1039–1056.
Dorale, J.A., Edwards, R.L., Ito, E., Gonzalez, L.A., 1998. Climate and vegetation history of the midcontinent from 75 to 25 ka: a speleothem record from Crevice Cave. Science 282, 1871–1874.

Dreybrodt, W., 2012. Processes in Karst Systems: Physics, Chemistry, and Geology. Springer Science & Business Media.
Dreybrodt, W., 2019. Kinetic fractionation of the isotope composition of 18O, 13C, and of clumped isotope 18O13C in calcite deposited to speleothems. Implications to the reliability of the 18O and Δ47 paleothermometers. Acta Carsol. 48 (3).
Dreybrodt, W., Buhmann, D., 1991. A mass transfer model for dissolution and precipitation of calcite from solutions in turbulent motion. Chem. Geol. 90, 107–122.
Dreybrodt, W., Scholz, D., 2011. Climatic dependence of stable carbon and oxygen isotope signals recorded in speleothems: from soil water to speleothem calcite. Geochim. Cosmochim. Acta 75 (3), 734–752.
Dreybrodt, W., Buhmann, D., Michaelis, J., Usdowski, E., 1992. Geochemically controlled calcite precipitation by CO_2 outgassing: field measurements of precipitation rates in comparison to theoretical predictions. Chem. Geol. 97, 285–294.
Dreybrodt, W., Eisenlohr, L., Madry, B., Ringer, S., 1997. Precipitation kinetics of calcite in the system $CaCO_3$–H_2O–CO_2: The conversion to CO_2 by the slow process $H^+ + HCO_3- \rightarrow CO_2 + H_2O$ as a rate limiting step. Geochim. Cosmochim. Acta 61, 3897–3904.
EL-Shenawy, M.I., Kim, S.T., Schwarcz, H.P., 2020. Carbon and oxygen isotope systematics in cave environments: lessons from an artificial cave “McMaster Cave”. Geochim. Cosmochim. Acta 272, 137–159.
Gabitov, R.I., Sadekov, A., Leinweber, A., 2014. Crystal growth rate effect on Mg/Ca and Sr/Ca partitioning between calcite and fluid: an in situ approach. Chem. Geol. 367, 70–82.
Guo, W., Zhou, C., 2019. Patterns and controls of disequilibrium isotope effects in speleothems: insights from an isotope-enabled diffusion-reaction model and implications for quantitative thermometry. Geochim. Cosmochim. Acta 267, 196–226.
Hammer, O., Dysthe, D., Jamtveit, B., 2007. The dynamics of travertine dams. Earth Planet. Sci. Lett. 256, 258–263.
Han, X., Fang, H., He, G., Reible, D., 2018. Effects of roughness and permeability on solute transfer at the sediment water interface. Water Res. 129, 39–50.
Jørgensen, B.B., Revsbech, N.P., 1985. Diffusive boundary layers and the oxygen uptake of sediments and detritus 1. Limnol. Oceanogr. 30, 111–122.
Kump, L.R., Arthur, M.A., 1999. Interpreting carbon-isotope excursions: carbonates and organic matter. Chem. Geol. 161, 181–198.
Levitt, N.P., Eiler, J.M., Romanek, C.S., Beard, B.L., Xu, H., Johnson, C.M., 2018. Near equilibrium 13C-18O bonding during inorganic calcite precipitation under Chemo-stat conditions. Geochem. Geophys. Geosyst. 19 (3), 901–920.
Liu, Z., Svensson, U., Dreybrodt, W., Daoxian, Y., Buhmann, D., 1995. Hydrodynamic control of inorganic calcite precipitation in Huanglong Ravine, China: field measurements and theoretical prediction of deposition rates. Geochim. Cosmochim. Acta 59, 3087–3097.
Lojen, S., Trkov, A., Ščančar, J., Vázquez-Navarro, J.A., Cukrov, N., 2009. Continuous 60-year stable isotopic and Earth-alkali element records in a modern laminated tufa (Jaruga, river Krka, Croatia): implications for climate reconstruction. Chem. Geol. 258, 242–250.
Mavromatis, V., Gautier, Q., Bosc, O., Schott, J., 2013. Kinetics of Mg partition and Mg stable isotope fractionation during its incorporation in calcite. Geochim. Cosmochim. Acta 114, 188–203.
Mickler, P.J., Stern, L.A., Banner, J.L., 2006. Large kinetic isotope effects in modern speleothems. Geol. Soc. Am. Bull. 118, 65–81.
Mook, W., Bommerson, J., Staverman, W., 1974. Carbon isotope fractionation between dissolved bicarbonate and gaseous carbon dioxide. Earth Planet. Sci. Lett. 22, 169–176.
Mucci, A., Morse, J.W., 1983. The incorporation of Mg^{2+} and Sr^{2+} into calcite overgrowths: influences of growth rate and solution composition. Geochim. Cosmochim. Acta 47, 217–233.
Osácar, M.C., Arenas, C., Auqué, L., Sancho, C., Pardo, G., Vázquez-Urbez, M., 2016. Discerning the interactions between environmental parameters reflected in δ13C and δ18O of recent fluvial tufas: lessons from a Mediterranean climate region. Sediment. Geol. 345, 126–144.
Oster, J.L., Montañez, I.P., Sharp, W.D., Cooper, K.M., 2009. Late Pleistocene California droughts during deglaciation and Arctic warming. Earth Planet. Sci. Lett. 288, 434–443.
Parkhurst, D.L., Appelo, C.A.J., 1999. User's guide to PHREEQC (version 2): a computer program for speciation, batch-reaction, one-dimensional transport, and inverse geochemical calculations. Water-Resour. Invest. 99 (4259), 312.
Plummer, L.N., Wigley, T.M.L., Parkhurst, D.L., 1978. The kinetics of calcite dissolution in CO 2-water systems at 5 degrees to 60 degrees C and 0.0 to 1.0 atm CO2. Am. J. Sci. 278 (2), 179–216.
Riechelmann, D.F.C., Deininger, M., Scholz, D., Riechelmann, S., Schröder-Ritzrau, A., Spötl, C., Richter, D.K., Mangini, A., Immenhauser, A., 2013. Disequilibrium carbon and oxygen isotope fractionation in recent cave calcite: comparison of cave precipitates and model data. Geochim. Cosmochim. Acta 103, 232–244.
Romanek, C.S., Grossman, E.L., Morse, J.W., 1992. Carbon isotopic fractionation in synthetic aragonite and calcite: effects of temperature and precipitation rate. Geochim. Cosmochim. Acta 56, 419–430.
Sulpis, O., Mucci, A., Boudreau, B.P., Barry, M.A., Johnson, B.D., 2019. Controlling the diffusive boundary layer thickness above the sediment–water interface in a thermostated rotating-disk reactor. Limnol. Oceanogr., Methods 17, 241–253.
Tang, J., Dietzel, M., Böhm, F., Köhler, S.J., Eisenhauer, A., 2008a. Sr2+/Ca2+ and 44Ca/40Ca fractionation during inorganic calcite formation: II. Ca isotopes. Geochim. Cosmochim. Acta 72 (15), 3733–3745.
Tang, J., Köhler, S.J., Dietzel, M., 2008b. Sr^{2+}/Ca^{2+} and $^{44}Ca/^{40}Ca$ fractionation during inorganic calcite formation: I. Sr incorporation. Geochim. Cosmochim. Acta 72, 3718–3732.
Turner, J.V., 1982. Kinetic fractionation of carbon-13 during calcium carbonate precipitation. Geochim. Cosmochim. Acta 46, 1183–1191.
Watkins, J.M., Hunt, J.D., 2015. A process-based model for non-equilibrium clumped isotope effects in carbonates. Earth Planet. Sci. Lett. 432, 152–165.
Watkins, J.M., Hunt, J.D., Ryerson, F.J., DePaolo, D.J., 2014. The influence of temperature, pH, and growth rate on the $\delta^{18}O$ composition of inorganically precipitated calcite. Earth Planet. Sci. Lett. 404, 332–343.
Yan, H., Sun, H., Liu, Z., 2012. Equilibrium vs. kinetic fractionation of oxygen isotopes in two low-temperature travertine-depositing systems with differing hydrodynamic conditions at Baishuitai, Yunnan, SW China. Geochim. Cosmochim. Acta 95, 63–78.
Yan, H., Schmitt, A.-D., Liu, Z., Gangloff, S., Sun, H., Chen, J., Chabaux, F., 2016. Calcium isotopic fractionation during travertine deposition under different hydrodynamic conditions: examples from Baishuitai (Yunnan, SW China). Chem. Geol. 426, 60–70.
Yan, H., Liu, Z., Sun, H., 2020. Large degrees of carbon isotope disequilibrium during precipitation-associated degassing of CO_2 in a mountain stream. Geochim. Cosmochim. Acta 273, 244–256.
Zavadlav, S., Rožič, B., Dolenec, M., Lojen, S., 2017. Stable isotopic and elemental characteristics of recent tufa from a karstic Krka River (South-East Slovenia): useful environmental proxies? Sedimentology 64, 808–831.
Zeebe, R.E., 2011. On the molecular diffusion coefficients of dissolved CO2, HCO3-, and CO32- and their dependence on isotopic mass. Geochim. Cosmochim. Acta 75 (9), 2483–2498.
Zeebe, R.E., Wolf-Gladrow, D.A., Jansen, H., 1999. On the time required to establish chemical and isotopic equilibrium in the carbon dioxide system in seawater. Mar. Chem. 65 (3–4), 135–153.
Zhang, J., Chen, F., Holmes, J.A., Li, H., Guo, X., Wang, J., Li, S., Lü, Y., Zhao, Y., Qiang, M., 2011. Holocene monsoon climate documented by oxygen and carbon isotopes from lake sediments and peat bogs in China: a review and synthesis. Quat. Sci. Rev. 30, 1973–1987.